

A semi-chronic motorized microdrive and control algorithm for autonomously isolating and maintaining optimal extracellular action potentials

Jorge G. Cham,¹ Edward A. Branchaud,¹ Zoran Nenadic,¹ Bradley Greger,² Richard A. Andersen,² and Joel W. Burdick¹

¹ Division of Engineering and Applied Science, California Institute of Technology, Pasadena, CA 91125

² Division of Biology, California Institute of Technology, Pasadena, CA 91125

Abstract

A system was developed that can autonomously position recording electrodes to isolate and maintain optimal quality extracellular signals. The system consists of a novel motorized miniature recording microdrive and a control algorithm. The microdrive was designed for chronic operation and can independently position four glass-coated Pt-Ir electrodes with micron precision over a 5mm range using small (3mm diameter) piezoelectric linear actuators. The autonomous positioning algorithm is designed to detect, align and cluster action potentials, and then command the microdrive to optimize and maintain the neural signal. This system is shown to be capable of autonomous operation in monkey cortical tissue.

1. Introduction

A fundamental challenge in experimental neurophysiology and the development of brain-machine interfaces is to record high quality action potentials from neuronal populations. Since the development of the recording electrode (Adrian 1926, Hubel 1957, Green 1958), two general approaches have emerged: acute and chronic recording methods. In acute recordings, individual electrodes are advanced into tissue at the beginning of each recording session through a cranial chamber, commonly by devices termed microdrives. The electrodes are advanced carefully until high quality neural activity is found. During the course of an experiment, readjustment of the electrode's position is often required to re-optimize and maintain signal quality. While this method allows the experimentalist flexibility in exploring different cell types, the process of signal optimization consumes a significant amount of time, even from an experienced operator. This is especially true for manual microdrives. Although motorized microdrives are commercially available (for example, Thomas Recording GmbH, Germany; FHC Inc., USA; Narishige Inc., Japan), the process of advancing the electrodes is still guided by human intuition, and it can be tedious or even impractical as the number of electrodes increases (Baker et al. 1999).

In chronic recordings, stationary multi-electrode assemblies, which are typically bundles or arrays of thin wires or silicon probes, are surgically implanted in the region of interest (for example, Porada, et al. 2000, Williams et

al. 1999, Rousche and Normann 1998). The signal yield of the implant array, i.e. the percentage of the array's electrodes that record active cells, depends upon the luck of the initial surgical placement. Moreover, small tissue migrations, inflammation, cell expiration or reactive gliosis can all cause subsequent loss of signal, thereby reducing or disabling the function of the recording array over time.

Chronic microdrives have been reported by several investigators. Variations of a common design in which manual turning of lead screws advances individual or small bundles of electrodes include Wall et al. (1967), Kubie (1984), Vos et al. (1999), Venkatachalam et al. (1999), Kralik et al. (2001), Tolia, et al. (2002) and Keating et al. (2002). Hoffman and McNaughton (2002) and deCharms et al. (1999) presented designs for chronic implants with large arrays of movable electrodes (49 and 144 respectively), in which a conventional microdrive is manually used to push or pull each electrode. Again, the amount of manual operation required to reposition each electrode in these devices can be impractical if not intractable. Moreover, it is difficult to ensure with such probes that specific neurons are tracked over time, as neuronal signals may be lost between adjustments. However, arrays with this many (or more) electrodes are likely to be needed for future working neuroprostheses. In this case, it is clearly not practical to require periodic manual adjustments of microdrives implanted on paralyzed patients.

Fee and Leonardo (2001) described a motorized chronic microdrive with two movable electrodes that is suitable for freely behaving small animals such as the zebra finch. This device, which uses two miniature electric motors, was still operated under human control. Fee and Leonardo reported that the ability to easily adjust the electrodes led to significant improvements in experimental productivity. This insight is promising for the activities of this paper that go beyond manual electrode adjustment to automated adjustment of multiple electrodes. Related work includes the stabilization of electrodes for intracellular recordings over a period of a few minutes by Fee (2000), and the control architecture for a commercial acute multielectrode microdrive by Baker et al. (1999), which autonomously advances electrodes until target cells are detected, at which point human operators optimize the signal. To date no miniature microdrive has been reported that can seek out, optimize and maintain extracellular action potentials in a fully autonomous fashion.

This paper describes a motorized microdrive that can autonomously position four independent electrodes and that is suitable for semi-chronic operation in monkeys. By the term semi-chronic, we mean that it can be used within a recording chamber for a period of a few weeks. We describe a novel microdrive design, which uses miniature piezoelectric linear actuators. The underlying theory for the autonomous algorithm used to control the device is only summarized here, and is described in more detail in Nenadic and Burdick (2004). Finally, we present experimental results including autonomous isolations of cells in monkey cortex.

The autonomous probe positioning algorithm can be implemented on a wide variety of devices. Additionally, the mechanical microdrive design can also be used as a conventional human-guided microdrive, and has the advantage of extremely small size. While the microdrive and control algorithm presented here are independent of each other, the system described in this paper serves as a test-bed for developing future "smart" neural recording implants that are fully autonomous. The full realization of the dream of a miniaturized chronically implantable autonomous electrode array will await further advances in micro-machine technology. In the short term, by reducing the amount of time required for an operator to isolate a cell, by allowing many cells to be isolated in parallel, and by maintaining high signal quality, autonomously operated microdrives can greatly increase the efficiency with which neurophysiological studies are conducted.

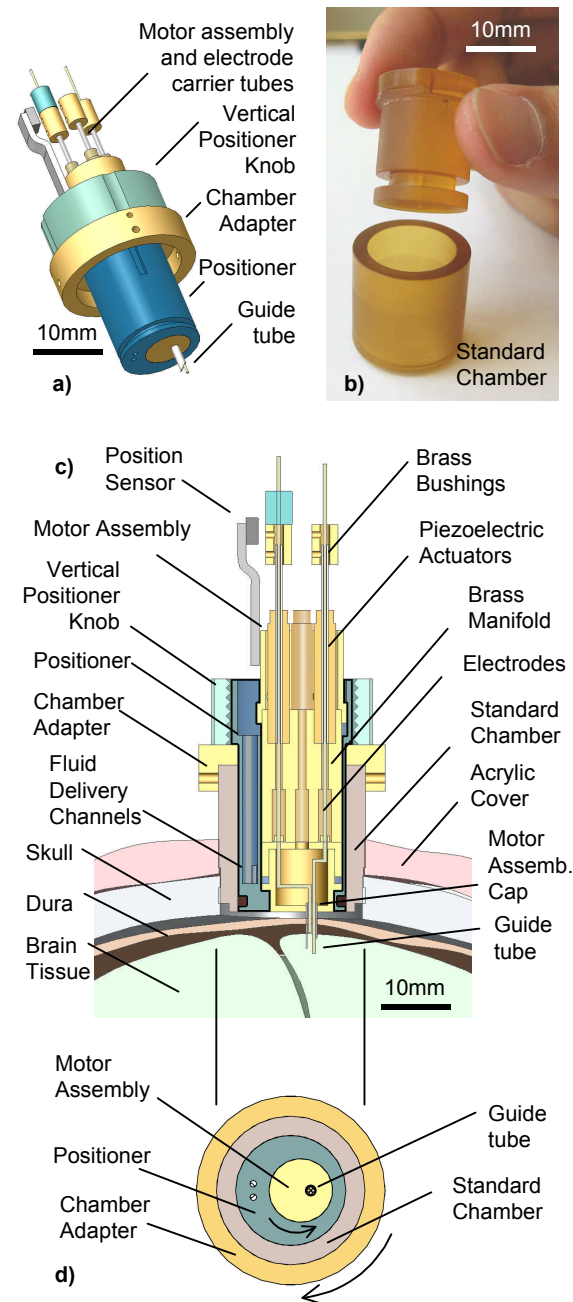


Figure 1. Design of the prototype microdrive. a) Rendered model of the design; b) standard cranial chamber used in laboratory; c) cross-section of the device inside of chamber, illustrating relative position to skull and brain tissue; d) front view of the device: rotation of the motor assembly and positioner allows X-Y positioning of the guide tube.

2. Methods

2.1 Motorized microdrive design

The basic design of our prototype is shown in Figure 1a. The prototype is designed to fit inside a standard laboratory cranial chamber, used for acute experiments in non-human primates, to allow semi-chronic operation. A semi-chronic design has the advantage that the device can be repositioned over a different region with minimal effort and without need for additional surgeries. The chamber, shown in Figure 1b, is a hollow plastic cylinder that is placed over a craniectomy and embedded in acrylic. The chamber can be sealed airtight using a cap, as shown in the figure.

As illustrated in Figure 1c, the device consists of a core motor assembly that fits inside a gross vertical and horizontal positioner. The positioner in turn is fitted inside the chamber through a chamber adapter. The motor assembly consists of four piezoelectric actuators, a cylindrical brass manifold and a cylindrical cap, as shown in the figure. A short guide tube emerges from the cap, with four inner channels spaced 500 microns apart through which the electrodes are lowered. This guide tube is off-center relative to the motor assembly, while the motor assembly and positioner are arranged as non-concentric cylinders. Rotation of both the motor assembly and the positioner adjusts the horizontal or X-Y position of the guidetube relative to the chamber over an 6mm diameter area, as shown in Figure 1d. The positioner is constrained to move only in the vertical direction relative to the chamber adapter by two slots on its sides that match two set screws on the adapter. This allows gross vertical or Z positioning of the electrodes by turning a knob that engages the outside threads at the top of the positioner, as shown in Figure 1c. Once the horizontal location of the guidetube has been determined and the device placed inside the chamber and lowered vertically by the positioner knob, set screws lock all the parts together, and the electrodes are then advanced by the actuators.

The electrodes are positioned by custom-made "Nanomotor" piezoelectric linear actuators (Klocke Nanotechnik, Germany, part NMSB0T10). The actuators, shown in Figure 2a, are 3mm in diameter and 22.5mm in length. These actuators were chosen for their accuracy (unloaded, they can be positioned with nanometer accuracy), high range of motion (5mm), relatively high force output (up to 0.03N of force), and direct linear drive (no gears or lead screws are needed to convert rotary to linear motion), thereby avoiding inaccuracies in positioning due to gearing backlash. The actuators are activated by a saw-

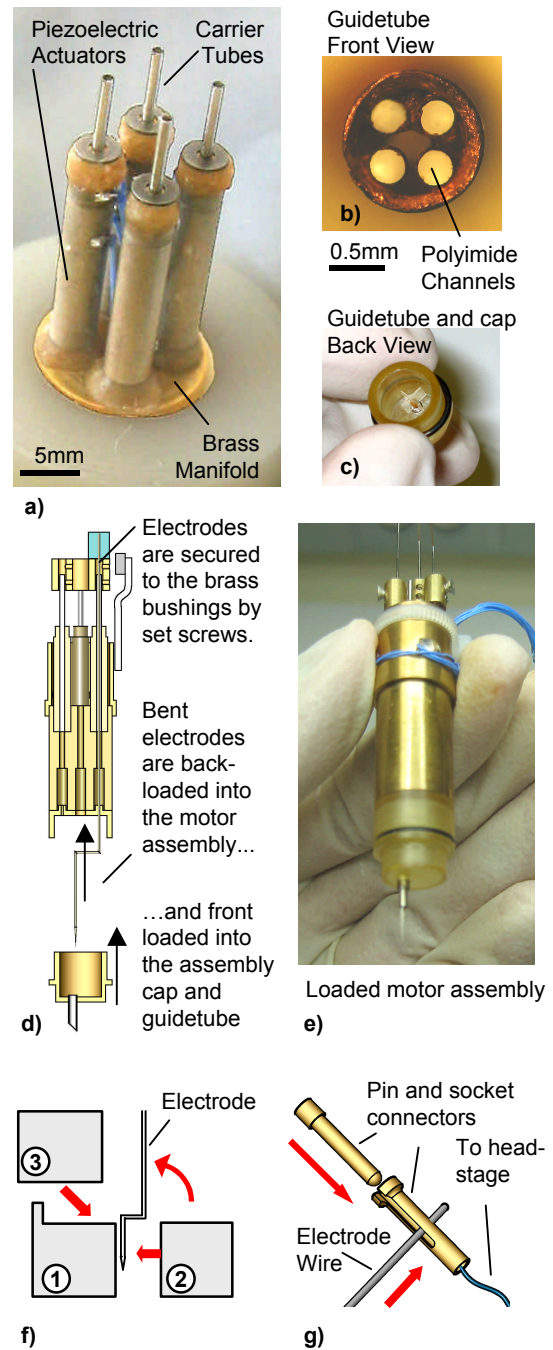


Figure 2. a) "Nanomotor" piezoelectric actuators; b) front close up of the guide tube, showing the four inner channels; c) back view of the motor assembly cap, showing the back of the guide tube; d) loading procedure for electrodes; e) loaded motor assembly; f) a jig that consists of three machined aluminum blocks that fit together allows electrodes to be bent at precise pre-determined locations; g) electrode connector.

tooth-shaped voltage signal with a minimum peak-to-peak amplitude of 30V. The frequency and amplitude of

the sawtooth wave determine the speed of positioning (maximum of approximately 2mm/s). The piezoelectric drives are mounted on a brass manifold that helps absorb the reaction forces that occur during activation of the drives. This prevents the motion of each drive from affecting the position of the others. In this design, the manifold increases the height and weight of the over-all device, though it may be possible to further reduce its size since its dimensions were chosen conservatively through direct experimentation by the actuator manufacturer.

The piezoelectric element in each actuator drives a hollow steel carrier tube through its center. Each electrode is passed through the center of one of these tubes and attached at the top to small brass bushings by set screws. The electrodes (FHC Inc., USA, part UE-RA1), are Pt-Ir wires (125 micron diameter), sharpened and glass coated a length of 5mm at the tip, and insulated by .008" OD polyimide tubing the rest of the length, with 10mm exposed at the end for electrical connection. Typical impedance is 1.5 to 3 MOhms at 1kHz. Each electrode is placed inside a 27ga steel tube, and the tube is pre-bent by 90 degrees in two locations such that one end is aligned with the actuator, and the sharpened end is aligned with the guide tube, as shown in Figure 2d. Since the guide tube is off-center to the carrier, each electrode must be bent a different amount. The electrodes and steel tube are bent using a custom-made system of jigs for accuracy and consistency, as shown in Figure 2f. A small length of the flexible coated wire is left between the bent tube and the electrode tip to allow for misalignments in assembly. The guide tube is made from hypodermic steel tubing (0.051" ID diameter) cut to size with four 0.012" ID .016" OD polyimide tubes arranged inside (see Figure 2b). The guide tube can be sharpened to penetrate thick dural tissue if necessary.

An alternate cap for the motor assembly can be used for single-electrode operation. This cap has a 23ga hypodermic stainless steel guide tube aligned with the piezoelectric motor drive, such that bending of the electrode is not necessary.

Electrical connection is made to the electrode by crimping the end of the wire between a pin and socket for D-sub-type connectors, to which a thin wire is soldered, as shown in Figure 2g. This wire is routed to a connector that carries the signal to a pre-amplifier.

A position sensor, shown in Figure 1c, was mounted on the device to track the movement of one of the electrodes for calibration and initial testing. The position sensor consists of a Hall-effect magnetic field sensor microchip

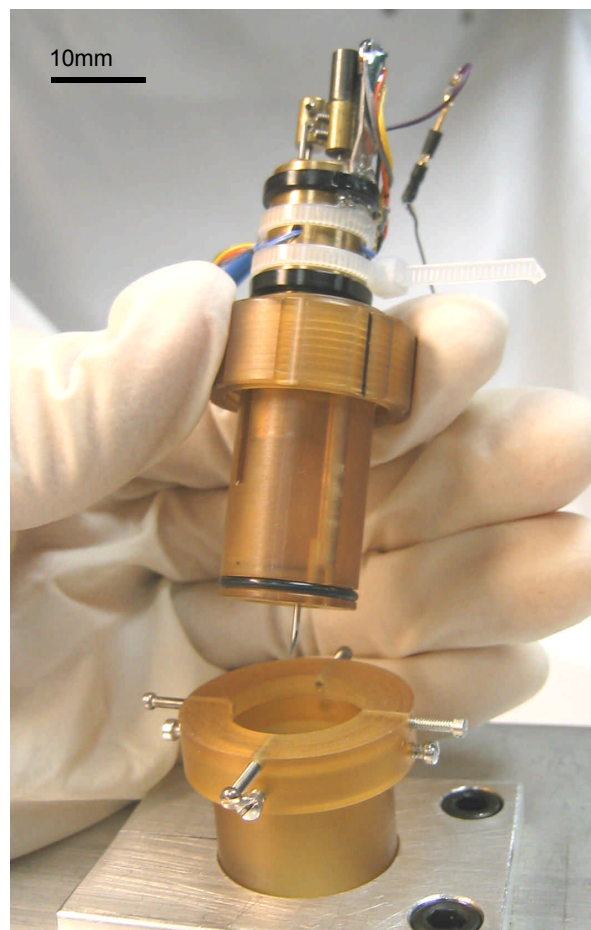


Figure 3. Assembled final prototype device and standard chamber.

(Micronas GmbH, Germany, part HAL401) and a small magnet attached to the brass bushing of the electrode drive. The output voltage of the sensor is proportional to its position relative to the magnet. This sensor is capable of sensing changes in position of one micron over a range of 5mm.

2.2 Microdrive fabrication and preparation

The chamber adapter, positioner, turning knob and parts of the motor assembly were machined from Ultem polyetherimide (McMaster Carr Supply Co., part 8686K76). This material matches the chamber material, and exhibits high temperature and chemical resistance, biocompatibility and machinability properties. Figure 2e shows a picture of the fabricated motor assembly, and Figure 3 shows the final prototype device. Engineering

drawings of the individual parts are shown in Figure 11. The overall device weighs approximately 40g.

Figure 2d shows how electrodes are loaded into the microdrive. After the electrodes have been placed inside the 27ga tubing and pre-bent using the jig system, they are first front-loaded into the cap of the motor assembly through the guide tube. This is facilitated by a small set of plastic cross plates, as shown in Figure 2c, which help guide the electrode tips into the individual polyimide channels inside the guide tube. Then, the electrodes and cap are attached to the rest of the motor assembly, back-loading the electrodes through the piezoelectric drive carrier tubes. For the single electrode configuration, the electrode is simply back-loaded into the guide tube, through the motor assembly, and attached at the top.

Movement of the piezoelectric microdrives was characterized and calibrated by observing and measuring its motion under a standard microscope. The actuators can be commanded to move one step by sending a single pulse of the sawtooth wave. At full voltage, the actuators move approximately one micron per commanded step. By reducing the voltage amplitude of the pulse, the step size could be observably reduced to 0.5 microns. While there is an offset between moving forwards and moving backwards that must be accounted for when commanding movements, the actuator movement is quite repeatable. This movement was tested in free air and in gelatin, and finally in animal cortex, showing only small variations (approximately 10%) in step size. Activation of each actuator did not cause any discernible unwanted vibrations of the electrodes and did not affect the motion of the other actuators.

2.3 Control Algorithm

Controlling a microdrive to isolate and maintain action potentials from active neurons *in vivo* is a difficult task even for experienced experimentalists. An autonomous control algorithm must not only discriminate and optimize action potentials in signals with significant noise levels, but must also deal with eventualities such as the presence of multiple cells, dying cells, cells with low firing rates and transient noise artifacts due to subject movements.

The basic architecture of the autonomous control algorithm for one electrode consists of two layers. The first layer is a state machine, which performs the initial search for action potentials, monitors the cell isolation and maintenance processes, and commands appropriate actions for the eventualities mentioned above. The second layer is the stochastic optimization method devel-

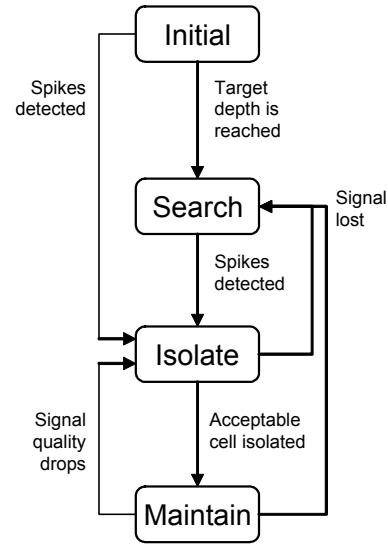


Figure 4. Simplified diagram of the autonomous algorithm state machine.

oped in Nenadic and Burdick (2004). This method optimizes signal quality in the presence of action potentials, given that only noisy observations are available.

A simplified diagram of the state machine is shown in Figure 4. At each state, the algorithm samples the neural signal for a short length of time (in this case, 20 sec) and searches for action potentials. Depending on the outcome, the state machine may execute a change of state and/or send a move command to the microdrive to reposition the electrode.

The system is started in the “Initial” state, once the microdrive device has been positioned over the desired recording region inside the chamber. The purpose of this initial state is to advance the electrode without frequent pauses to sample the signal, since initial positioning of the microdrive may place the electrodes up to several millimeters from the desired recording region. Electrodes are advanced 250 microns (at a velocity of 4 microns per second) between samples until one of the following events occur: either a previously determined target depth is reached, which can be obtained from anatomical data such as MRI scans (Scherberger et al., 2003), or until action potentials are detected in the neural signal.

Action potentials are detected using the unsupervised wavelet-based detection method presented in Nenadic and Burdick (2004). Traditional methods such as amplitude and power thresholding, window discrimination and matched filtering require human supervision and experience, as they depend on the amplitude, shape and phase

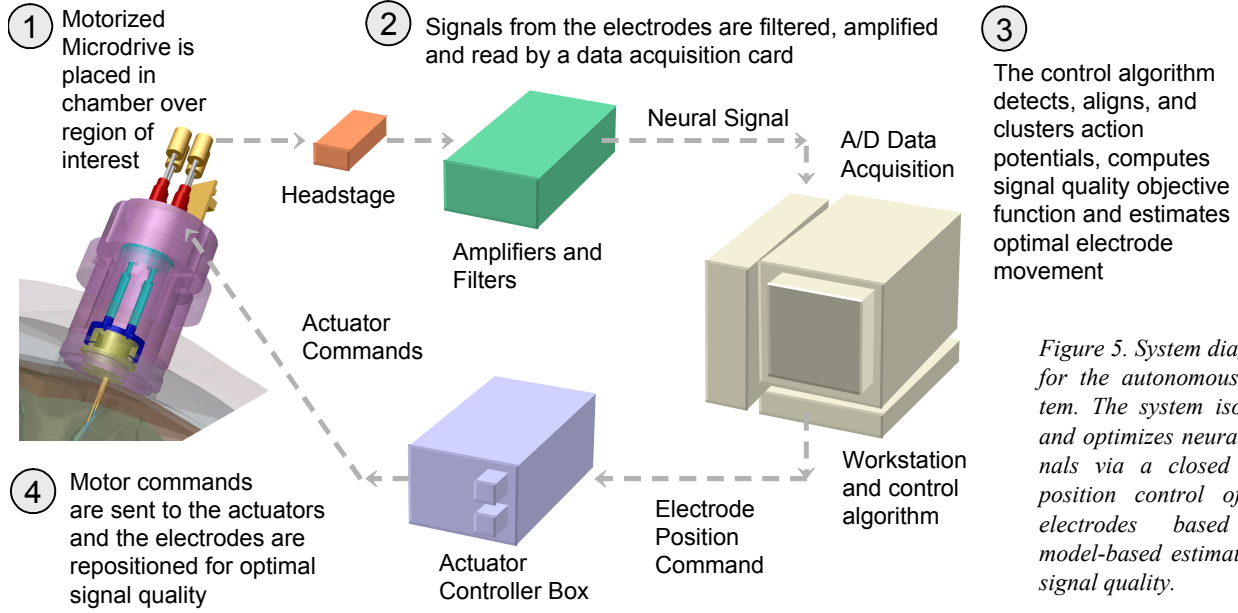


Figure 5. System diagram for the autonomous system. The system isolates and optimizes neural signals via a closed loop position control of the electrodes based on model-based estimates of signal quality.

of the action potentials recorded, which can change as the electrode moves relative to the cell body. The wavelet-based method is better suited for unsupervised operation because its detection threshold is independent of spike shape and phase, and can be set beforehand as a trade-off between spike omission and false alarms. This method has been shown to give consistent performance over a wide range of signal-to-noise ratios and firing rates. Action potentials are considered to be present only when the number of events detected by the method exceeds a minimum firing rate, in this case 2Hz. Once detected, action potentials are aligned and clustered using the correlation method and finite mixture model clustering method described in Nenadic and Burdick (2004).

If the target depth is reached without detection of action potentials, the algorithm switches to the “Search” state, which advances the electrode only 50 microns (at 4 microns per second) between samples. If action potentials are detected while in the “Initial” or “Search” states, the system switches to the “Isolate” state.

The goal of the “Isolate” state is to reposition the electrode to maximize signal quality. In the method of Nenadic and Burdick (2004), this goal is mathematically formalized by defining a (non-negative) objective function over a segment of a real line in the neighborhood of the cell (since the electrode is constrained to linear motion). The resulting curve is called the “cell isolation curve”, and the goal is to find the position that maximizes it. The method presented here is independent of the exact choice of objective function, but it must capture some

measure of signal quality. In this paper, we test the use of two different metrics, though others are certainly possible. The first metric tested is the peak-to-peak amplitude (PTPA) of the recorded action potentials. The second metric is the distance in principal component space (DPCS) between a useful cell and confounding cells or noise, which may be useful in the presence of multiple spiking neurons.

Since only noisy observations of the objective function are available, the objective is defined as a regression function,

$$M(x) = E(y|x) \quad (1)$$

where y is the chosen measure of signal quality, x is the position of the electrode along its range of motion and $E(\cdot)$ is the expectation operator. Normally, gradient descent methods may be applied to find the maximum of this function. However, estimating the gradient directly from noisy local observations can be numerically unstable. Instead, we estimate the regression function itself with a set of basis functions, using all (or a subset of) the previous observations obtained at the preceding electrode positions. For simplicity, we choose a polynomial basis function of the form:

$$\hat{M}(x, n, B) = \sum_{i=1}^n b_i x^{(i-1)} \quad (2)$$

where x is electrode position, $B = [b_1, b_2, \dots, b_n]^T$ are the polynomial coefficients, and n is the order of the

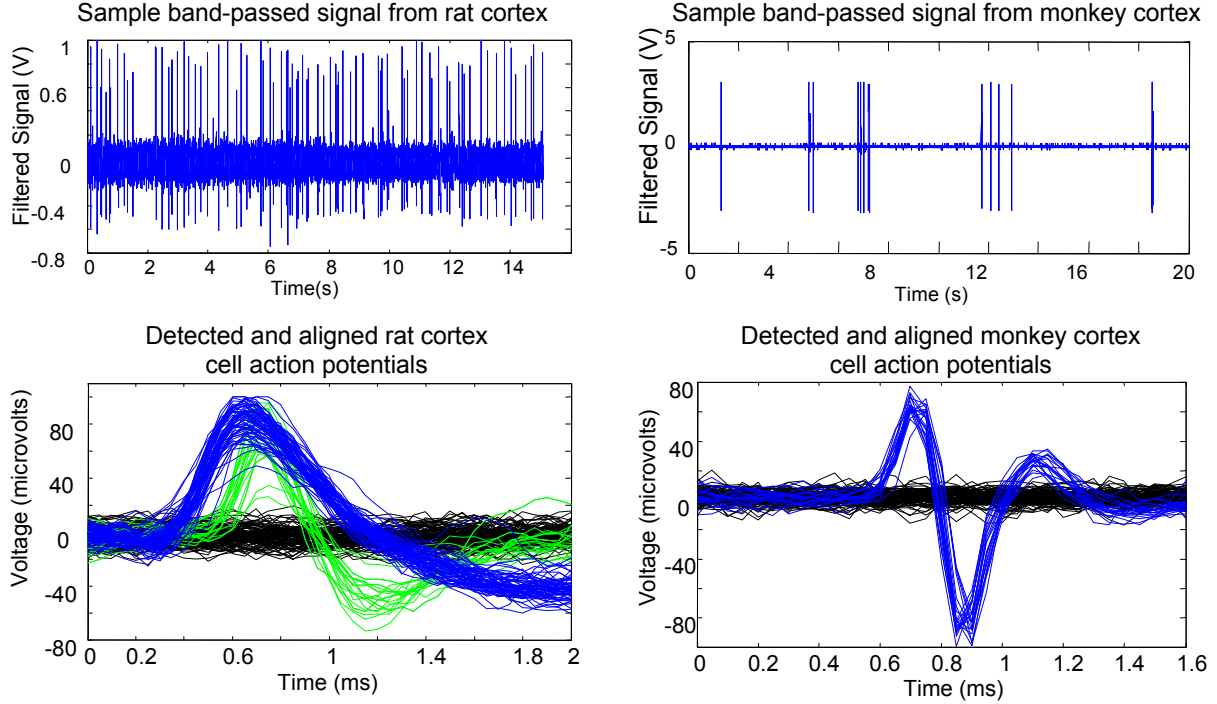


Figure 6. Filtered neural signals obtained with the microdrive in rat and monkey cortex.

model. The order of the model is adaptively chosen through Bayesian theory. For each model order up to a maximum (in our case, 5th order), the posterior probability of that model given the observed data is computed and the model order that maximizes this probability is then chosen. Once the order is determined, the parameters B are found through the maximum likelihood method (ML), which, in this case, reduces to the linear least square method (LLS).

Once an estimate of the objective function is obtained, the algorithm moves towards the maximum using a form of Newton's method:

$$x_{k+1} = x_k + C|H_k|^{-1}\xi_k \quad k = k_0, k_0 + 1, \dots \quad (3)$$

where x_{k+1} and x_k are the positions of the electrodes at iterations $k+1$ and k , respectively, $C > 0$ is an appropriately chosen scale factor, and H_k and ξ_k are estimates of the Hessian and first derivative of $M(x)$ at x_k respectively. The gradient and Hessian are computed explicitly from formulas of the first and second derivatives of Equation 2.

Initially, the "Isolate" state moves the electrode in constant increments (in our case, 20 microns) between samples of the neural signal. The basis function

approximation and Newton's method optimization are used only after enough observations of the regression function have been collected. This is necessary because the Bayesian formulation assumes that the number of observations is greater than the highest model order considered for the approximation. Otherwise, overfitting might occur. In our case, the algorithm verifies two conditions before the basis function approximation is considered valid. First, it checks that a minimum number of observations k_0 have been collected (in our case, this number is 5). Second, if enough observations have been collected then the most likely model order must be greater than 1 (meaning a horizontal straight line). If either of these conditions is not met, the algorithm continues sampling the space in constant increments. If both conditions are met, the optimization process proceeds according to Equation 3.

The state machine remains in the "Isolate" state until either an upper bound on signal quality is reached, or it is determined that the maximum of the regression function has been reached. The first criterion prevents the algorithm from driving the electrode into the body of a cell that lies directly in its path. This upper bound must be chosen large enough that spiking information can be discerned, but small enough that the electrode will be kept at a safe distance from the cell. In our case, it is defined as a

form of signal-to-noise ratio (SNR) as the amplitude of the detected spikes divided by the root mean square of the “noise” (recorded signal with the spikes subtracted). For the second criterion, the algorithm is determined to have reached the maximum of the regression function when the commanded step size from Equation 3 reaches a minimum value, in this case 1 micron, which will occur when the gradient approaches zero. If the maximum value that is realized is below a lower bound of signal quality, then the cell isolation is considered unacceptable, and the algorithm switches back to the “Search” state. In the experiments presented in this paper, we tested various values of the upper and lower bound SNR, finding best results with values of 12 and 8 respectively.

If the cell is considered isolated, the state machine changes to the “Maintain” state. In this state, the algorithm samples the neural signal while keeping the electrode stationary. This continues until the measured signal quality falls below the acceptable SNR level. Once this occurs, the cell is no longer considered isolated, and the algorithm switches back to the “Search” state in order to re-acquire the signal.

A significant problem occurs when the firing rate of a cell being isolated is intermittent, or the cell stops firing altogether, especially in the presence of other nearby cells. Such situations can create extreme outliers in sampling that can confound the isolation algorithm. This eventuality was remedied by increasing the recording time at each sample. This time was set to 20 seconds, which allowed activity from intermittent firing cells to be captured consistently. The threshold for determining the presence of an active cell was an average firing rate of 2Hz over the 20 second sample period. If, while tracking a cell in the “Isolate” or “Maintain” state, the firing rate drops below this threshold, the signal is sampled at that position one more time before determining that the cell is no longer present and resetting to the “Search” state once again.

2.4 Experiment setup and procedure

Initial experiments were performed on anesthetized rats to test the basic operation of the microdrive and control algorithm. The rats were anesthetized with isoflurane, administered ketamine (1ml/Kg, IP) and atrophine (0.05ml, subcutaneously) and prepared for surgery. Once anesthetized, the rats were held in a stereotaxic rig via ear bars and mouth piece, and administered isoflurane accordingly to maintain sedation while heart and temperature were monitored. A small craniectomy was performed over the barrel cortex region, and the microdrive

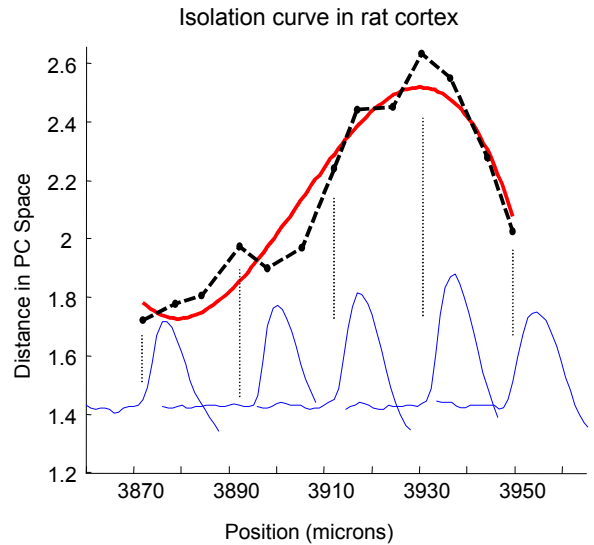


Figure 7. Isolation curve recorded from rat cortex. The dashed line shows the measured signal quality as a function of electrode position with sample spike forms (solid blue lines) at different positions indicated by the dotted lines. The solid red line shows the fitted basis function approximation.

was suspended over the craniectomy using a stereotaxic arm. The electrodes were then lowered under operator control through dura and into cortical tissue using the piezoelectric motors in both multiple and single-electrode drive configurations.

Single-electrode experiments were conducted in the posterior parietal cortex (Andersen and Buneo, 2002) of an awake, behaving adult macaque monkey. The microdrive was installed in the cranial chamber at the beginning of each recording session. Using the vertical positioning knob, the device was lowered by hand to a target depth. The algorithm was then activated and the system operated autonomously, using the PTPA metric. The monkey performed simple saccade (eye movement) tasks in a darkened room during the experiments. The animal care and handling in these experiments were in accord with the guidelines of the National Institutes of Health and have been reviewed and approved by the local Institutional Animal Care and Use Committee.

Between recording sessions, the electrodes were removed from the microdrive and sterilized, and the microdrive was disassembled and cleaned with alcohol. Typical microdrive assembly and disassembly times were 20-25 minutes by an experienced operator with good manual dexterity. Alcohol was also sometimes applied to the junction between the piezoelectric element and the carrier tube of the actuators before each recording session

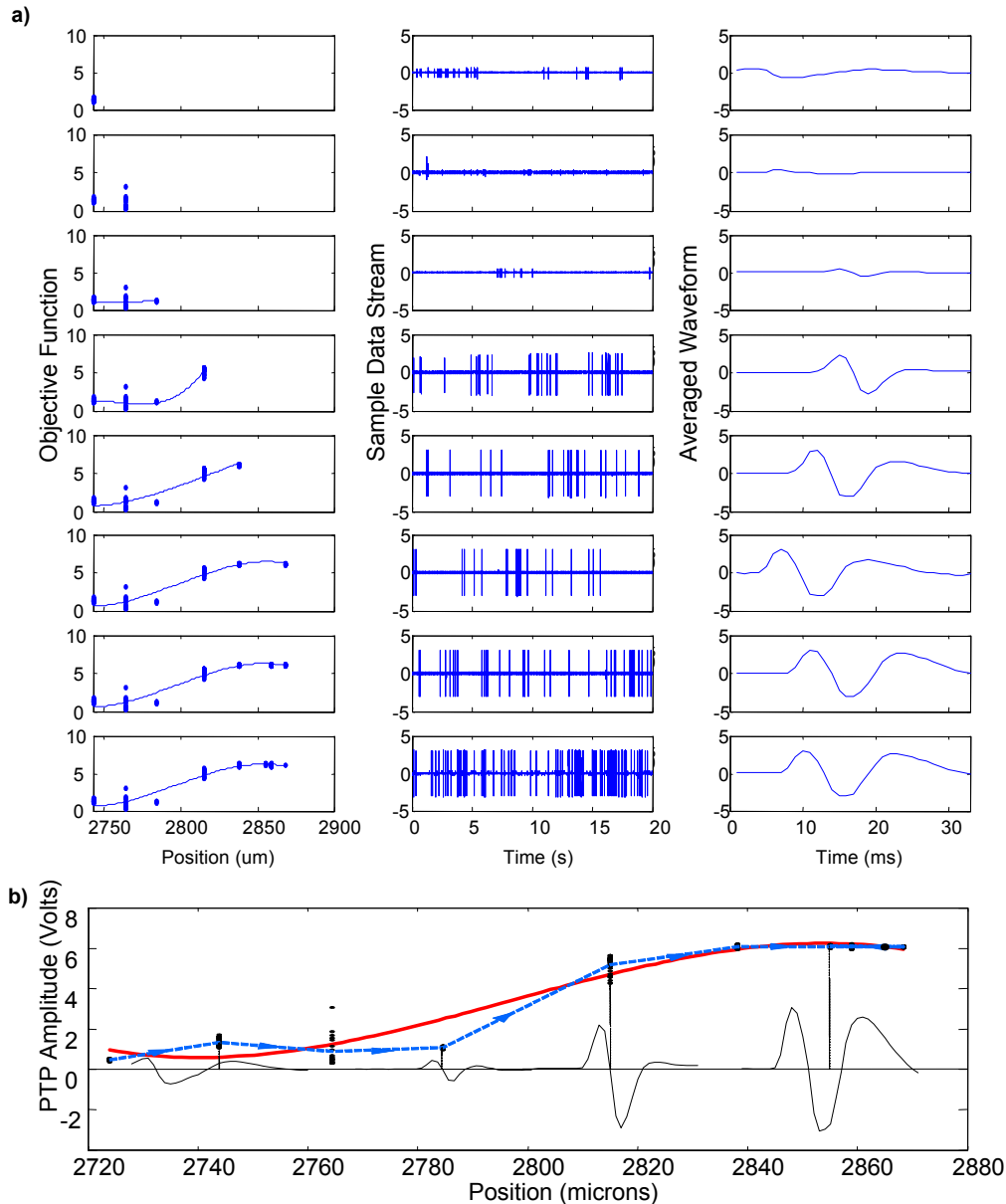


Figure 8. Cell Isolated in monkey cortex using the autonomous semi-chronic microdrive system. a) Progression of algorithm in presence of action potentials. The left column shows snapshots of the sampled objective function and the basis function approximation; the middle column shows the signal spike train; the right column shows the averaged waveform of the detected spikes. b) Final isolation curve and average spike waveforms at each position. In this case, the signal was optimized until the maximum of the isolation curve was found.

to clear out any small debris or viscous biological liquid that impeded motion.

A diagram of the autonomous system is shown in Figure 5. The output of the electrode from the microdrive was connected to a DAM-80 (World Precision Instruments Inc., USA) headstage and amplifier in the rat experiments, and to a Plexon (Plexon Inc., USA) headstage and amplifier in the monkey experiments. The sig-

nal output from the amplifiers in both setups was recorded by a data acquisition card (National Instruments Inc., USA). Filter and gain settings varied with experimental conditions and objectives. A faraday cage was used to shield the set up from ambient noise in the rat experiments. The carrier tubes of the actuator were connected to ground (they are electrically insulated from the actuator signal) to provide additional shielding to the electrode. The piezoelectric motors were powered and

activated by a controller purchased with the actuators (Klocke Nanotechnik, Germany, part NWC). The position sensor was powered by a standard 5V power supply, and its output also read by the data acquisition card. The control algorithm was implemented in Matlab (Mathworks Inc., USA).

3. Results

The motorized microdrive in single-electrode configuration and the control algorithm were used to record from neurons in rat and monkey cortex. Sample filtered neural signals obtained with the microdrive in rat and monkey cortex are shown in Figure 6. The top plots show raw data streams bandpass filtered between 300Hz and 10kHz for the rat and monkey. The bottom plots show the detected, aligned and clustered spikes from their respective data streams using the detection and alignment methods previously discussed. Figure 7 shows sample results from rat cortex. Shown in the figure is signal quality (in this case measured by the DPCS metric) as a function of electrode position, with the corresponding averaged spike shapes at each position. These results demonstrate the presence of our conceptual isolation curves in rat cortex, which are the basis of our autonomous algorithm.

Figure 8 shows a sample result of autonomous cell isolation in monkey cortex. In this case, the algorithm was initiated after the microdrive was installed in the chamber and allowed to operate autonomously without human intervention. The algorithm first advanced the electrode in the “Initial” and “Search” states for over 1.5mm until faint spike activity was detected. Shown in Figure 8a is the sequence of steps taken by the algorithm once the state machine transitioned to the “Isolate” state. The first column shows the positions of the electrode and the measured objective function (in this case, PTPA). The second column shows the corresponding data stream at that position, and the third column shows the average spike waveform. As shown, the algorithm first advanced the electrode in constant increments. After enough observations were made to allow an adequate model to be fitted, the polynomial fit was made, shown as a solid line. Once a peak in the objective function was detected, the control algorithm repositioned the electrode toward the optimal location. The sequence ended when the cell was determined to be isolated by the algorithm, as per the minimum step size criteria previously discussed. Figure 8b is a concatenated plot of the sequence, showing the final isolation curve approximation (solid line), the progression of the algorithm (dotted line) and the average waveforms.

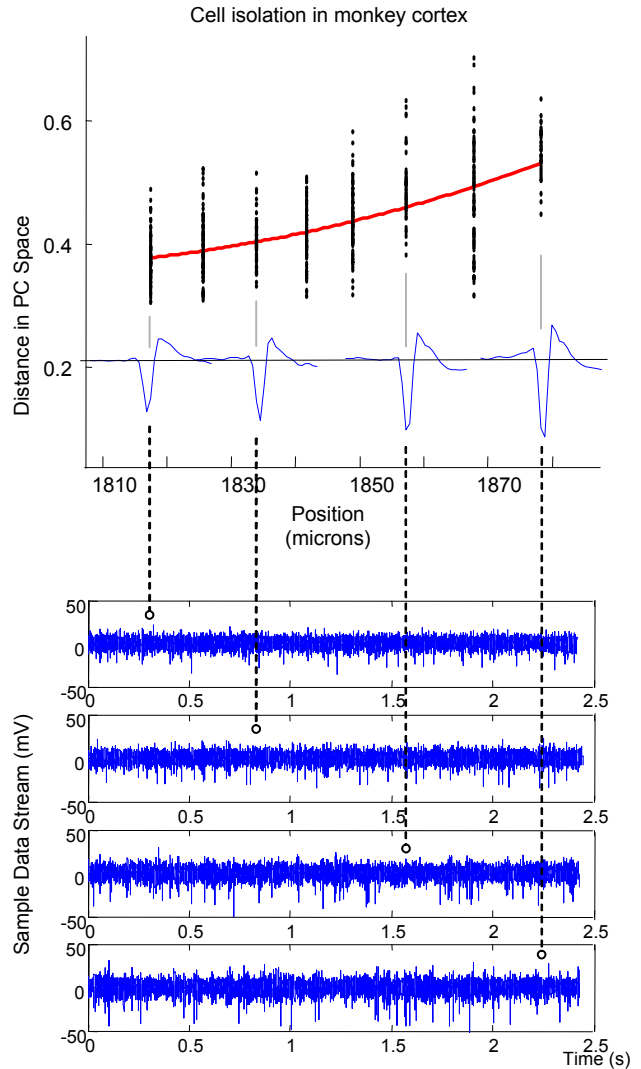


Figure 9. Cell isolated in monkey cortex using the autonomous semi-chronic microdrive system. In this case, the cell was considered to be isolated when the signal quality reached a maximum value, in order to avoid potential damage to the cell. The top plot shows the sampled signal quality (in black) and the fitted regression function (in red) as a function of electrode position, with average action potentials shown for four different positions. The data streams that correspond to the four positions are shown below (in blue), with correspondence indicated by the dashed lines.

The results from Figure 8 illustrate the potential risk of unconstrained signal maximization. As shown, the firing rate of the cell increased as the electrode moved forward, indicating that the electrode was affecting cell behavior possibly due to very close proximity. Figure 9 shows final results of the algorithm in monkey cortex in which the upper bound on SNR was implemented, in order to prevent potential damage to the cell. In this case, the

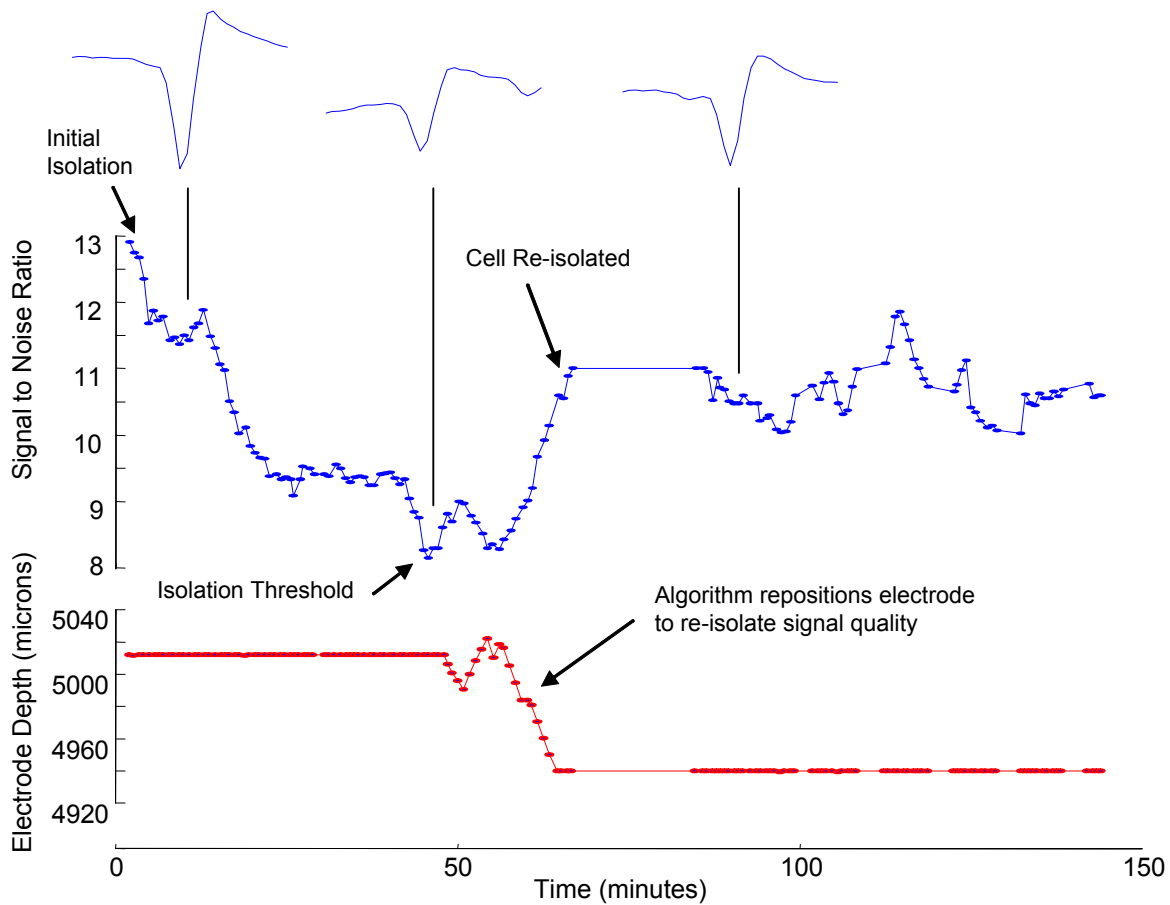


Figure 10. Time history of signal quality over a period of 2.5 hours, after the cell was isolated by the autonomous algorithm. The figure shows how signal quality slowly degraded, perhaps due to tissue migration. Once signal quality degraded below a minimum threshold, the autonomous algorithm repositioned the electrode to reacquire an acceptable signal quality level.

algorithm advanced the electrode to maximize the regression function until the upper bound was reached, at which point the cell was considered isolated.

To date, ten cells have been isolated with the autonomous system in monkey cortex. Cells have been isolated and maintained for up to 3 hours. Figure 10 shows a sample time history of signal quality after the cell has been determined isolated by the algorithm and the state machine entered the “Maintain” state. As shown, signal quality (measured by the SNR) degrades over time, possibly due to tissue migration. Once the signal dropped below the lower bound SNR threshold, the algorithm automatically re-initiated the search and isolation processes and reacquired the signal. The continuous measurements of the PTPA metric shown in the figure and the consistency of the spike shape provide evidence that the same cell was being tracked throughout the entire experimental session.

4. Discussion

4.1 Motorized microdrive design

The novel miniature motorized microdrive was shown capable of advancing and retracting electrodes in cortical tissue with micron precision and recording high-quality neural signals. The electro-mechanical design of the microdrive addresses several issues in recording implant design. First, the overall device is of minimal size and weight so that it does not significantly affect behavior in awake non-human primates and can be implanted semi-chronically (for several days or weeks at a time). Many of the commercially available motorized microdrives such as the ones mentioned in the introduction use relatively large actuators and are meant only for acute experiments.

stroke of the actuators also makes them well suited to this application, since a range of motion of several millimeters, if not centimeters, is often required depending on the depth of the target structure, and the accuracy of the implantation procedure. In addition, the inherent linear motion of the actuators reduced the amount of careful assembly necessary and did not require the design of a lead screw transmission. Gears and lead screws can often introduce a significant amount of imprecision in the drive due to gearing backlash. Such hysteresis can result in instability or inaccuracy in the control algorithm. In general, the actuators were tolerant to significant handling and electrode loading and unloading. The drive mechanism of the actuators can be sensitive to friction due to misalignment or viscous liquids, reducing the force output and requiring careful attention in assembly and maintenance.

The microdrive was tested in both multiple and single electrode configurations. Typical signal-to-noise ratios of spike amplitude were 8-10, and as high as 15. With proper shielding and grounding, the electronic noise generated by the idle actuators was on the same order of magnitude as ambient and 60Hz noise from surrounding equipment, and did not significantly impact signal quality. During motion of the electrodes, the actuators generated noise that saturated the electrode signal. However, since the control algorithm requires that the signal be sampled at discrete positions, simultaneous motion and recording was not necessary.

The microdrive performed well over several dozen recording sessions without sign of performance degradation. The device is rugged in construction, safe and relatively easy to install in the head chamber and to reload and maintain electrodes. Careful attention must be paid when front-loading the electrodes into the device, as the fragile electrode tips can be easily damaged.

4.2 Control algorithm

The algorithm presented in this paper was shown to autonomously command the microdrive to seek and isolate action potentials from cells. All of the different methods used in the isolation algorithm, from spike detection, alignment and clustering to regression function model selection and estimation, require no supervision and account for the stochastic nature of the task. The results shown for monkey cortex were obtained with no human intervention once the microdrive was placed inside the chamber.

The algorithm and isolation results presented were for one electrode. Interference in the form of tissue move-

ments between multiple movable electrodes is possible, however, and strategies for coordinating the movement of multiple electrodes will have to be developed.

While the stochastic optimization method of Nenadic and Burdick (2004) is deeply rooted in theory, the heuristic-based state machine architecture allows for flexibility in dealing with unpredictable eventualities common in recording environments in behaving animals. Many of the state transitions for dealing with eventualities are based on common practices by experienced human experimentalists. Although the basic implementation presented here was shown to work in the monkey, the exact heuristics and values used by the state machine may need to be fine-tuned for particular experimental conditions such as subject species, brain region and type of cell targeted in order for the autonomous algorithm to perform optimally.

4.3 Autonomous system

The novel microdrive and the algorithm presented here do not necessarily need to be implemented together. The microdrive design provides a working device for acute or semi-chronic recordings that can be controlled by a human operator, or by an alternate control algorithm. Similarly, the algorithm can be used to control other microdrives for autonomous operation. The successful integration of the two systems, however, is presented as a first step towards future “smart” neural implants that are fully autonomous. Such autonomous implants could contribute to the efficiency and flexibility of neurophysiological studies by freeing the experimentalist from time-consuming tasks such as frequent implantation surgeries and finding and maintaining high-quality neural signals.

5. Acknowledgements

We thank the members of the Andersen lab at Caltech, especially Daniella Meeker, Bijan Pesaran, Boris Breznen, Sam Musallam, Kelsie Pejsa and Lea Martel. Thanks also to Aimee Eddins and Rodney Rojas for help in fabricating the prototype. This work was funded by NIH, DARPA, the Boswell Foundation, ONR and NSF.

6. References

- Andersen RA and Buneo CA. Intentional maps in posterior parietal cortex. *Ann.Rev. Neurosci* 25: 189-220, 2002.
- Adrian E. The impulses produced by sensory nerve endings. *J Physiol* 61: 49-72, 1926.
- Baker SN, Philbina N, Spinks R, Pinchesa EM, Wolperta DM, MacManusb DG, Pauluisc Q and Lemon RN. Multi-

- ple single unit recording in the cortex of monkeys using independently moveable microelectrodes. *J. Neuroscience Methods* 94: 5-17, 1999.
- deCharms RC, Blake DT and Merzenich MM. A multielectrode implant device for the cerebral cortex. *J Neurosci Methods*, 93: 27-35, 1999.
- Fee MS and Leonardo A. Miniature motorized microdrive and commutator system for chronic neural recording in small animals. *J Neurosci Methods* 112: 83-94, 2001.
- Fee MS. Active stabilization of electrodes for intracellular recording in awake behaving animals. *Neuron* 27: 461-468, 2000.
- Gray CM, Maldonado PE, Wilson M and McNaughton B. Tetrodes markedly improve the reliability and yield of multiple single-unit isolation from multi-unit recordings in cat striate cortex. *J Neuroscience Methods* 63: 43-54.
- Green J. A simple microelectrode for recording from the central nervous system. *Nature* 182: 962, 1958.
- Hoffman KL and McNaughton BL. Coordinated Reactivation of Distributed Memory Traces in Primate Neocortex. *Science* 297: 2070-2073, 2002.
- Hubel D. Tungsten microelectrode for recording from single units. *Science* 125: 549-550, 1957.
- Keating JG and Gerstein GL. A chronic multi-electrode microdrive for small animals. *J Neurosci Methods* 117: 201-206, 2002.
- Korshunov VA. Miniature microdrive for extracellular recording of neuronal activity in freely moving animals. *J Neurosci Methods* 57:77-80, 1995.
- Kralik JD, Dimitrov DF, Krupa DJ, Katz DB, Cohen D and Nicolelis MAL. Techniques for long-term multisite neuronal ensemble recordings in behaving animals. *Methods* 25: 121-50, 2001.
- Kubie JL. A Driveable bundle of microwires for collecting single-unit data from freely-moving rats. *Physiology & Behavior* 32: 115-118, 1984.
- Lemon R. Methods for neuronal recording in conscious animals. Pages 18-37, 1984.
- Nenadic Z, Burdick JW. Autonomous electrode positioning for optimization of extracellular recordings. *IEEE Trans Biomedical Eng*, submitted, 2004.
- Nenadic Z, Burdick JW. Spike detection using the continuous wavelet transform. *IEEE Trans Biomedical Eng*, in press, 2004.
- Normann RA, Maynard EM, Rousche PJ and Warren DJ. A neural interface for a cortical vision prosthesis. *Vision Research* 39: 2577-2587, 1999.
- Porada I, Bondar I, Spatz WB and Kruger J. Rabbit and monkey visual cortex: more than a year of recording with up to 64 microelectrodes. *J Neurosci Methods* 95: 13-28, 2000.
- Rall W. Electrophysiology of a dendritic neuron model. *Biophys. J.* 2: 145-167, 1962.
- Rousche PJ and Normann RA. Chronic Recording Capability of the Utah Intracortical Electrode Array in Cat Sensory Cortex. *J. Neurosci. Meth.*, 82:1-15 (1998).
- Scherberger H, Fineman I, Musallam S, Dubowitz DJ, Bernheim KA, Pesaran B, Corneil BD, Gilliken B, and Andersen RA. Magnetic resonance image-guided implantation of chronic recording electrodes in the macaque intraparietal sulcus. *J Neurosci Methods* 130:1-8, 2003
- Strumwasser F. Long-term recording from single neurons in brain of unrestrained mammals. *Science* 127: 469-470, 1957.
- Tolias AS, Siapas AG, Smirnakis SM, Logothetis NK. Coding visual information at the level of populations of neurons. Program No. 557.5. 2002 Abstract Viewer/Itinerary Planner. Washington, DC: Society for Neuroscience, 2002.
- Venkatachalam S, Fee MS and Kleinfeld D. Ultra-miniature headstage with 6-channel drive and vacuum-assisted micro-wire implantation for chronic recording from the neocortex. *J Neurosci Methods* 90: 37-46, 1999.
- Vos BP, Wijnants M, Taeymans S and De Schutter E. Miniature carrier with six independently moveable electrodes for recording of multiple single-units in the cerebellar cortex of awake rats. *J Neurosci Methods* 94: 19-26, 1999.
- Wall PD, Freeman J, Major D. Dorsal horn cells in spinal and in freely moving rats. *Exp Neurol* 19: 519-529, 1967.
- Williams JC, Rennaker RL and Kipke DR. Long-term neural recording characteristics of wire microelectrode arrays implanted in cerebral cortex. *Brain Research Protocols* 4: 303-313, 1999.